

## LIQUID BRIDGES AND FLOATING ZONES

by I. Martínez<sup>1</sup> and A. Cröll<sup>2</sup>

<sup>1</sup>Universidad Politécnica, E.T.S.I. Navales, E-28040-Madrid

<sup>2</sup>Kristallographisches Institut, Albert-Ludwigs-Universität Freiburg, D-7800 Freiburg

### ABSTRACT

A liquid bridge spanning between two sharply-edged coaxial solids represents a fluid interface configuration of the highest interest, both to basic fluid science and to material science, particularly as a model of the molten bridge in the floating-zone technique of crystal growth and high melting point refining. In this presentation, the fluidmechanical aspects of this modelling are considered, and some results of its application to the real processing of silicon rods are presented.

Keywords: capillarity, floating zone, liquid bridge, microgravity, experimental, crystal growth.

### 1. INTRODUCTION

One important problem in research on advanced materials is the behaviour of the silicon melt during the floating-zone process of crystal growth. The practical interest on this problem is so great (the major part of the highest-purity electronic and photonic materials is presently obtained using this technique), and the advantage of experimentation under microgravity so unique (larger floating zones unmasked by gravity forces can be realised), that its combination has motivated by itself the arousal of a widespread effort in the scientific and technical community to better understand this multidisciplinary problem.

The key characteristic of this method is that the molten zone does not need to be in contact with a foreign solid (crucible) that, besides being awkward to achieve (the working temperature must be well above the 1690 K of the melting temperature of silicon), would introduce impurities (molten silicon is a most reactive material) unacceptable for the applications envisaged.

Although it is a very crude simplification, one may distinguish in this problem between material-science-oriented research and fluid-science-oriented research, according to whether the interest is centred on the final product (grown silicon crystal) or on understanding the processing details.

The present article is aiming primarily to this second aspect of the problem: fluid science research on floating zones, and more specifically to the mechanical stability of the liquid bridge model. Both the floating zone and the liquid bridge are held by surface tension and wetting forces (capillarity), spanning between two sharply-edged coaxial solids against the natural tendency of liquids to adopt a spherical shape in absence of other forces, and the tendency to creep down the rod in a gravity field or to spill out due to shocks, vibration or

rotation of the supporting rods or of the atmosphere surrounding the bridge if not in vacuum (it is customary to work in an inert-gas atmosphere or saturated with one of the melt species if it has a high vapour pressure, as when GaAs is processed).

### 2. THE FLOATING ZONE PROCESS

The objective of the first silicon floating-zone (FZ) experiments in space (performed during the first Spacelab flight FSLP (Refs. 1 and 2) and the TEXUS 7 sounding rocket flight (Ref. 3) was to investigate the cause of dopant striations in FZ silicon. Comparison of the  $\mu\text{g}$  crystals with their terrestrial counterparts showed that similar striation patterns, although with less variation in dopant concentration, were formed. Similar results were obtained by  $\mu\text{g}$  experiments dealing with the directional solidification of a silicon sphere (Refs. 4 and 5). The conclusion was that Marangoni convection and not buoyancy convection is mainly responsible for the formation of striations in FZ silicon. These results were corroborated by experiments with a confined melt zone, where the silicon was coated by a thin (5  $\mu\text{m}$ ) film of silica glass to suppress Marangoni convection (Refs. 6 and 7). Such crystals showed no dopant striations, i.e. Marangoni convection is the only cause for the formation of striations, at least with the zone dimensions (diameter,  $D=8+10$  mm, length,  $L=12+15$  mm) and averaged temperature gradients (35+95 K/cm) employed.

The configuration used aboard TEXUS (Spacelab) is as follows. The sample to be processed is a perfectly cylindrical silicon rod of 8 mm (10 mm) in diameter and 90 mm (130 mm) long, machined from larger crystals obtained on Earth by the Czochralskii (CZ) or the floating-zone (FZ) technique. The silicon rod is, on a macroscopic scale, uniformly doped with phosphorus or antimony to some 50 parts per million (i.e.  $6.10^{17}$   $\text{cm}^{-3}$ , or 4  $\text{mol/m}^3$ ); the uniformity is achieved by dopant diffusion enhanced by high temperature soaking. For the TEXUS experiments, the sample is placed inside a fused quartz ampoule (held at the ends and with a gap at the lateral walls) pressurised with an inert gas.

The sample is placed inside a mirror furnace (ELLI for TEXUS, MHF for Spacelab) as sketched in Fig. 1, and it is heated appropriately by means of halogen lamps in the focus of the ellipsoids in order to create a molten zone, floating between the unmolten ends of the rod by capillary forces, and the furnace is displaced axially relative to the rod in order to make the molten zone travelling along the rod.

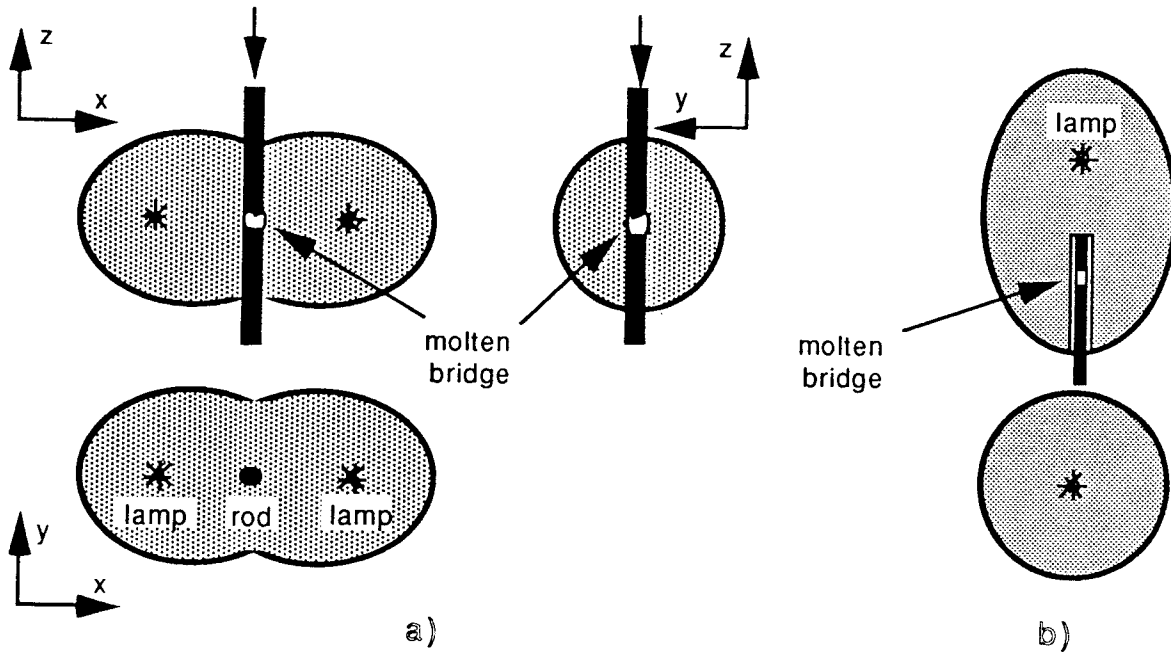


Fig. 1. Mirror furnaces used to grow silicon crystals in space: a) three views of the double-ellipsoidal Mirror Heating Furnace (MHF) used aboard Spacelab; b) two views of the single-ellipsoidal furnace ELLI used aboard TEXUS sounding rockets.

To increase the economic value of the processed rod, its diameter  $D$  should be as large as possible, but the height  $L$  of the molten zone is coupled to its diameter through the heating process (it is not possible to inject heat deeply inside without it spreading laterally), what normally means that the molten zone must be more slender than a square cylinder, that is, its height  $L$  must be larger than its diameter  $D$ . Thus, the slenderness  $\Lambda$ , defined by:

$$\Lambda \equiv \frac{L}{D} = \frac{L}{2R} = \frac{L}{R_1 + R_2} \quad (1)$$

(where the latter is applied for the case of unequal size of the supports) is bound to be larger than unity.

But on Earth, the gravitational field prevents liquid bridges and floating zones to be higher than a few millimetres, as can be estimated by balancing the hydrostatic head  $\Delta\rho gL$ , where  $\Delta\rho$  is the density difference between the liquid and the surrounding atmosphere, with a capillary pressure of the order  $\sigma/L$ ,  $\sigma$  being the interfacial tension (force per unit length). The nondimensional group that relates this two effects is called the Bond number, here written as  $Bo_L$  to pinpoint the difference with the more usual definition in terms of the radius,  $Bo_R$ :

$$Bo_L \equiv \frac{\Delta\rho gL^2}{\sigma}, \quad Bo_R \equiv \frac{\Delta\rho gR^2}{\sigma} \Rightarrow Bo_L = 4\Lambda^2 Bo_R \quad (2)$$

We first consider floating zone processing in space, in absence of gravity, because it seems to be the simplest case. As the heat is applied to the surface of the melt and removed via the solid ends, heat transfer inside the melt dictates that the molten zone is shorter at its centre than at the free surface, that is, there would be some solid caps protruding into the liquid section. Care should then be exercised during the processing

in order not to let the two protruding caps to touch each other, because this will produce polycrystalline growth. Besides, if the two solid ends were counterrotating (what is sometimes imposed to uniformize the temperature field) the forces associated to the mechanical coupling might endanger the driving mechanism.

Moreover, there is another complication and it is the fact that single crystals grow with a constant specific angle between the melt slope and the solidifying lateral profile, what is called receding angle  $\gamma$  (see detail in Fig. 2) that for silicon is  $\gamma=11^\circ$ . Is for this reason that the processing in space produces initially a reduction of the growing diameter (Fig. 2a) until the corresponding bulging in the melt (by mass conservation) restores the initial diameter of growing. It is this last stationary configuration that is studied the most.

On Earth, hydrostatic pressure forces the melt to adopt an amphora-like shape (Fig. 2b), so that if the processing is done upwards the  $11^\circ$  of the receding angle can be achieved from the beginning, thus simplifying in some way the processing.

In practice, to avoid the limitation to diameters of a few millimetres implied by the above reasoning, the needle-eye technique sketched in Fig. 2c is used on Earth to grow crystals up to 100 mm in diameter. The heating element on Earth is normally an electric coil that generates induction currents in the conducting melt (besides the heating effect there is some electromagnetic levitation effect that also helps to hold the liquid bridge).

From the several techniques to diagnose the perfection of the grown crystal (either on ground or in space) we concentrate on the measurement of the dopant distribution, what is best performed with the electrical spreading resistance technique, which measures the electrical resistance between two specifically conditioned probes separated some 10  $\mu\text{m}$  to

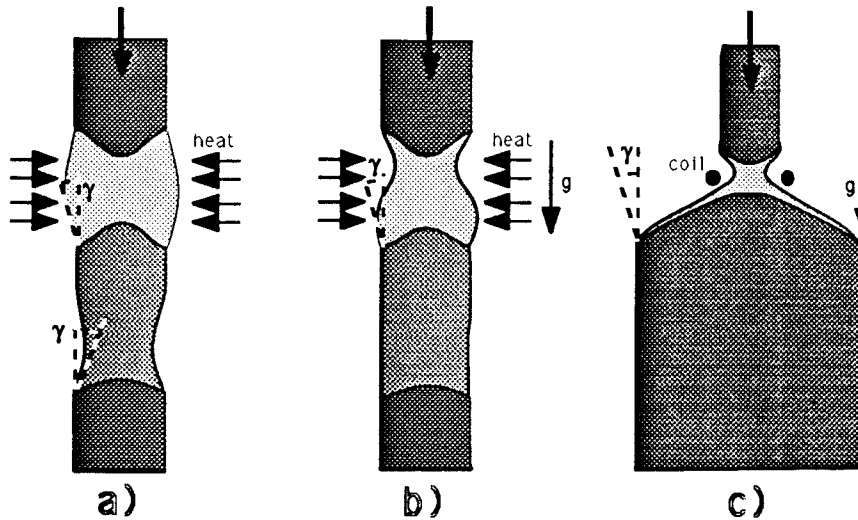


Fig. 2. Sketches of the floating zone process: a) processing in space produces an initial necking and afterwards a bulging melt; b) processing on Earth produces an amphora-like melt; c) processing on Earth using the needle technique of growth with widely different diameters.

20  $\mu\text{m}$ . The electrical resistance is very sensitive to dopant concentration and a good spatial resolution is achieved. The analysis of dopant distribution (also called segregation) shows the following [7]:

- There are concentration inhomogeneities both on the crystals grown in space and on ground.
- There are two types of inhomogeneities: macroscopic (also called macrosegregations, having a characteristic length  $L_c \gg 1 \mu\text{m}$ ) which are influenced by bulk motion and microscopic (also called microsegregations or striations<sup>1</sup>, with  $L_c \approx 1 \mu\text{m}$ ) which are caused by transient (oscillatory or turbulent) motion.
- Changes in macrosegregations can be correlated to bulk motions imposed by rotating the rod (or the crucible in the CZ technique) or arising from buoyancy or thermocapillary forces.
- Microsegregations (striations) can also be generated by rotation, and can be suppressed by covering the free surface with a thin layer of oxide ( $\text{SiO}_2$ ) that has a higher melting point but becomes plastic at the working temperatures. A hole larger than 1 mm in the coating already gives rise to striations. There is little influence of gravity on striations (only that the amplitude of the concentration ripple is slightly smaller under  $\mu\text{g}$ ), and despite its surface driven origin, the motion permeates to the whole zone. The critical Marangoni number for the onset of time-dependent thermocapillary convection has been determined experimentally to be in the order of 100+200 (Ref. 7).
- Electromagnetic fields may damp time-dependent motions and decrease striations.
- Stationary magnetic fields damp time-dependent motions and decrease striations: There are almost no striations visible in Si-crystals of 8 mm diameter (zone length  $\approx 10$  mm, axial temperature gradient  $\approx 35$  K/cm) grown in an axial magnetic field of 0.5 T.

A simple model can predict the nominal dopant distribution in

1. This time-dependent striations are called of type I, to distinguish them from those due to the growing kinetics, which are called of type II.

an ideal case, if one introduces the following simplifications:

- One-dimensional geometry, so that a perfect cylindrical melt is considered instead of the bulging or amphora-like shapes of Fig. 2.
- Quiescent configuration, so that no motion is considered (either thermocapillary or buoyant).
- Mass diffusivities in the solids are neglected, so that dopant concentration cannot be varied once it has solidified.
- Mass diffusivities in the liquid are large, so that the liquid composition can be assumed uniform, although in real crystal growth there is always a solute boundary layer with a buildup of dopant near the solidification front.
- Thermodynamic equilibrium conditions apply to the solidification front but not to the melting front, so that the ratio of concentrations at the solid and liquid sides of the solidification front can be assumed constant (the segregation coefficient implied by the equality of the chemical potential of the species at both phases).

With the above model the evolution of the FZ process would be as depicted in Fig. 3.

However, the real result bears little resemblance. An axial concentration profile corresponding to a silicon rod processed on Earth is presented in Fig. 4. Some radial concentration profiles can also be found in Ref. 7.

To end this section on the FZ process, a recent proposal for an experiment on the MAXUS sounding rocket is described.

The setup and the procedure of the  $\mu\text{g}$  experiment will be similar to those of the previous silicon FZ experiments on TEXUS, which were performed in the module TEM-02 "ELLI".

The sample consists of a doped (P or Sb) silicon single crystal of approx. 8 mm diameter and 90 mm length, mounted wall-free in a closed fused silica ampoule filled with 1 atmosphere of Ar 6N (99,9999% pure); see Fig. 5. The ampoule is centred and fixed in a steel adaptor, which can be directly mounted onto the translation and rotation mechanism of the mirror

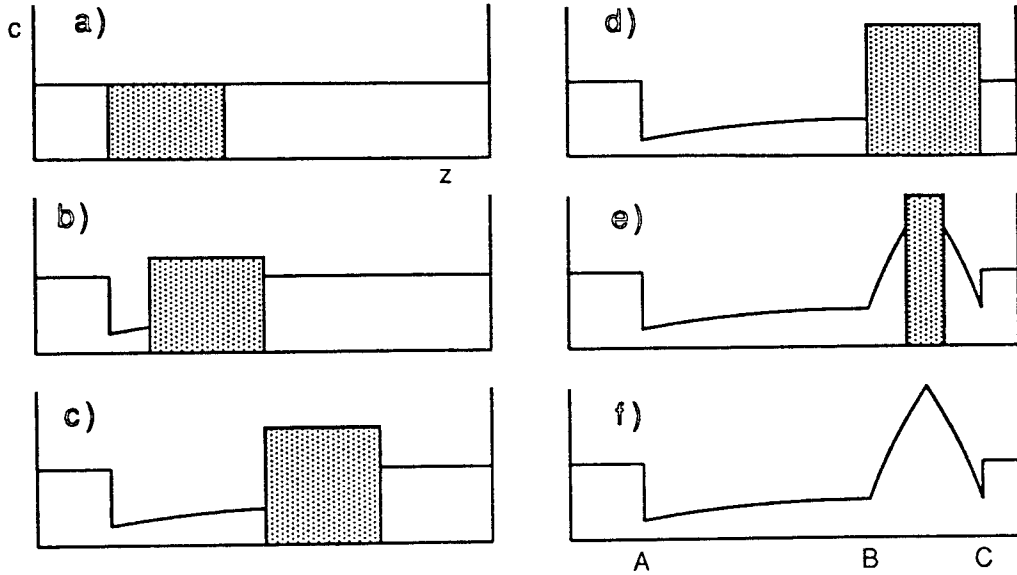


Fig. 3. Sketch of the ideal floating-zone processing showing the axial dopant-concentration profile,  $c$ , versus axial position,  $z$ , at several time instants (a, b, c, d, e, f). Section A corresponds to the first solidification front position (where processing starts), and B and C correspond to the last position of the molten zone (d) before switching-off the heating and the rapid solidification that follows, sketched in (e) and (f).

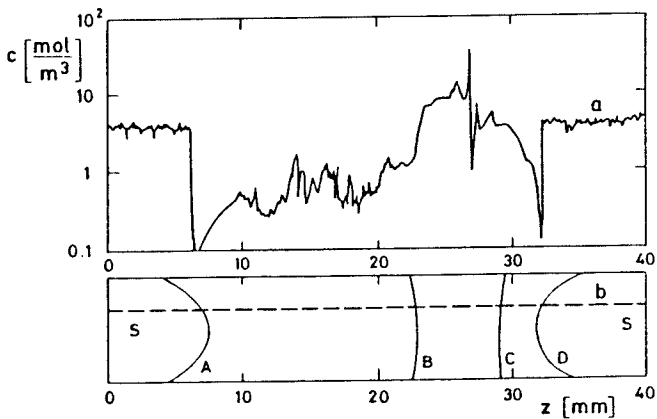


Fig. 4. Experimental measurement of the axial dopant-concentration (by the electrical spreading resistance technique) on a silicon rod of 8 mm in diameter and 90 mm in length (40 mm shown) initially doped with 50 ppm ( $4 \text{ mol/m}^3$  or  $6.10^{17} \text{ atom/cm}^3$ ) of antimony and processed on Earth. a, dopant concentration profile; b, line of measurement in the meridian section; s, unprocessed rod; A, first solidification front; B and C, last solid-liquid fronts before cooldown; D, final meeting of the fronts.

furnace. Based on the experience of the previous TEXUS experiments and the results of the computer simulations of the zone shape using the liquid bridge model, an operational profile as sketched in Fig. 6 will be evaluated by ground experiments in the flight module. Prior to lift-off the sample is preheated but not melted; during lift-off the lamp has to remain switched-off to prevent destruction of the filament. At the beginning of the microgravity phase, the sample is overheated to ensure rapid melting. Then the power is reduced to a lower value until the desired zone dimensions and steady-state conditions are achieved. Afterwards, the translation (5 mm/min) is started. During growth the zone shape is observed via realtime TV and controlled by telecommand of the lamp power.

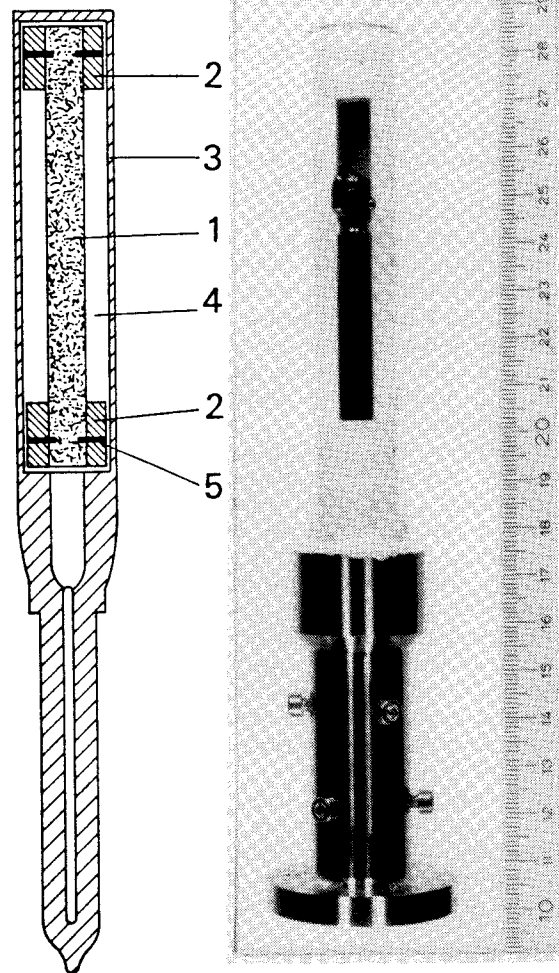


Fig. 5. TEXUS ampoule used for silicon rod processing by floating zone technique: a) sketch, b) ampoule in its support. 1, silicon rod of 8 mm diameter and 90 mm length; 2, fused silica rings; 3, fused silica ampoule; 4, argon gas; 5, tungsten pins.

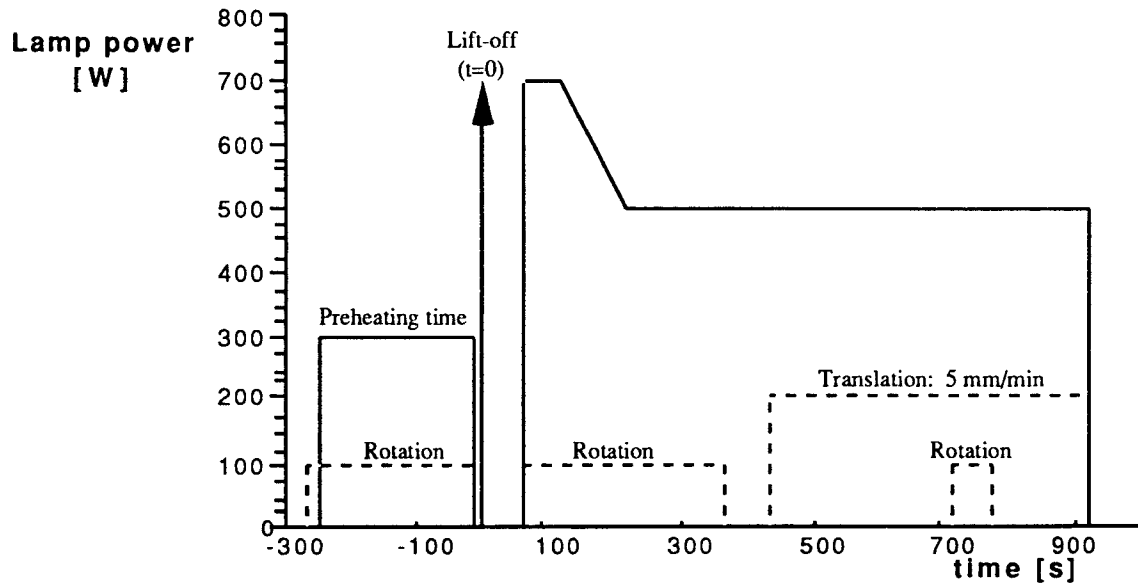


Fig. 6. Operations profile for the proposed silicon FZ experiment aboard the MAXUS sounding rocket.

To achieve the desired degree of control of the zone length, a longer time than in the previous TEXUS experiments (1 minute) will be necessary until the melt zone is fully established and stable. Therefore the 15 min experiment time on MAXUS will be preferred, allowing a time of about 6-7 min for thermal equilibration before crystal growth is started. The longer experiment time will also allow to recrystallise more material (and/or to use a lower translation rate), resulting in a more accurate determination of segregation. It might be possible to perform the experiment on TEXUS (with an estimated equilibration time of 2-3 min and a growth time of 3 min), but with an inevitable loss of accuracy concerning the control of the zone length and the analysis of segregation.

As mentioned above, realtime TV is necessary for the observation of the zone, preferably with two cameras placed at an angle of  $90^\circ$  (colour TV is not necessary). In addition, a photo-camera is also required for the analysis of the exact zone shape after the flight.

To determine the temperature profile in the zone (under 1g), a special measuring ampoule containing a Pt/PtRh thermocouple embedded in the crystal will be used. This ampoule exists and has already been used for the preparation of the TEXUS 22 experiment in 1989.

### 3. FROM FLOATING ZONES TO LIQUID BRIDGES

Although the protruding solid ends (solid caps entering into the liquid section) have a major impact on the logistics of the heating and pulling laws during real floating zone processing, they have minor importance for the internal motion (because it is surface driven) and no importance at all for the mechanical stability of the melt, so that, the liquid bridge model sketched in Fig. 7 is used instead of the real molten zone of Fig. 2; the similarities and differences between the two can be summarised as follows:

#### Statics:

-The liquid bridge is assumed to be at complete thermodynamic equilibrium, whereas if the solid-liquid interface for the melt were in the true thermodynamic

equilibrium it could be in any position, because it is indifferently stable. In practice, in the FZ, the solid-liquid interface is fixed by application of a non-uniform temperature field, slightly heating the melt and cooling the supports over and below the fusion temperature, respectively. If the temperature difference is not large, fluid properties (surface tension and density) can be taken as constant.

-Even during actual processing, where temperature differences of 100 K in 1 cm may exist, the variation of properties with temperature and the motions it creates are so mild (Ref. 8) that the outer shape and its mechanical

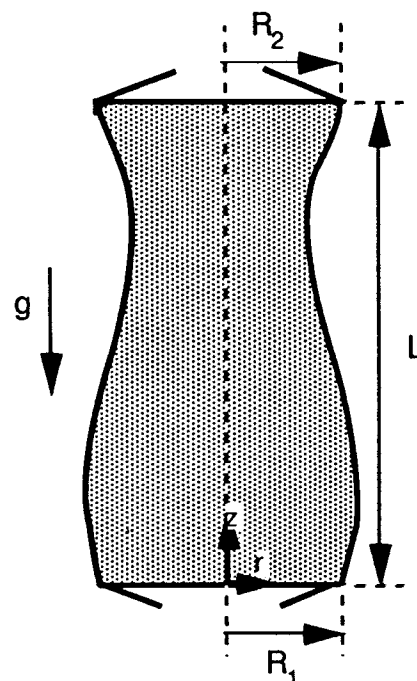


Fig. 7. Geometry of the liquid bridge used as a fluid science model of the floating zone sketched in Fig. 2.

stability seem to coincide with those predicted by the constant-property liquid bridge quiescent model.

- The problem of how good the model is in the description of the liquid-solid interaction is another issue. Because mechanical relaxation times are much shorter than thermal or diffusional ones, it can be anticipated that if the melt is suddenly shaken, the solid-liquid interfaces would remain the same (at least for short times). Does the liquid remain edge-attached to the solid, or does it slip over the solid? Experiments show that the anchoring assumption is correct (Ref. 9).

#### Dynamics:

- The interest is on predicting the eigenfrequencies and motions caused by imposed mechanical perturbations. The parameters that enter into the dynamic model of the liquid bridge (leaving aside geometry) are: surface tension, density and viscosity, and there is an ample choice of model fluids which show similar properties to those of the high temperature melts of interest. The same remark on boundary conditions as above apply.

#### Convection:

- The interest is on thermocapillary convection, and besides the dynamical parameters mentioned above, thermal diffusivity and temperature derivative of surface tension play the major role. A handicap of the model is that Prandtl numbers  $Pr = \nu/a$  (the ratio of viscous to thermal diffusivity) for melts of technological interest are of order  $Pr \approx 10^{-2}$  whereas for transparent liquids it is  $Pr \approx 10$ , that is three orders of magnitude different (see Table 1).
- Despite the deep penetration of surface driven convection in the zone (Ref. 7), it has been demonstrated that the onset of oscillatory motions is not affected by the presence of the feeding hole and the sealing O-ring in one of the discs (Ref. 10).
- In any case, it must always be kept in mind that the variation of surface tension with temperature is very difficult to measure for real melts (near 2000 K) and uncertainties even in the order of magnitude exist.

#### Diffusion:

- Although the study of segregation and transport of impurities is one of the major goals of experiments on the

floating zone process, little effort has been paid up to now to its analysis using the liquid bridge model (with a binary liquid).

#### Phase changes:

- This is genuine to the floating zone, and the liquid bridge model is assumed to not account for phase changes. However, using model substances as succinonitrile, which has a well-defined fusion point  $T_f = 330$  K, or even sodium nitrate ( $T_f = 580$  K), both of which have transparent melts, will surely help to understand real floating zone processing at 2000 K.

#### Electric and magnetic effects:

- Electric and magnetic fields are applied in real floating zone processes to better control the shape or the internal motions in the melt, and they can be similarly applied to the liquid bridge (Ref. 11), although the parametric characterisation needs further work.

#### Reactive processes:

- It is easily understandable that, working at 2000 K, every system must be considered reactive. For the same reason, it is difficult to think of a liquid bridge at 300 K as a good model to analyse chemical reactions of interest to the floating zone process, although the fact that a liquid bridge offers a highly controllable and free configuration will no doubt stimulate its use for chemical reaction research (f.i. the burning of a long cylindrical liquid column can only be achieved in this way).

The cylindrical liquid column presents the simplest geometry, except for the spherical drop, but the inconveniences in handling the latter renders the former to the foreground; this is why so many papers and experimental work have appeared since the opportunities to carry out experiments in microgravity platforms became a reality.

Coming back to what a FZ experimenter would like to learn by means of the LB model (Ref. 12), the following may be a summary in increasing order of complexity:

- How the outer shape of a given molten material evolves when certain pulling law  $S(t)$  and heating law  $Q(t)$  are applied; that is, he wants to know:

Table 1  
Properties of some important liquids on floating zone or liquid bridge research

Material	Si (at $T_f$ )	Ge (at $T_f$ )	Water (at 298 K)	DMS 5 (at 298 K)
Properties				
Melting Temperature, $T_f$ [K]	1690	1210	273	
Refractive Index at $\lambda = 0.6 \mu\text{m}$ , $n$	opaque	opaque	1.33	1.40
Density, $\rho \times 10^{-3}$ [kg.m <sup>-3</sup> ]	2.53	5.5	1	0.92
Thermal Expansion, $\alpha \times 10^3$ [K <sup>-1</sup> ]	0.14	0.10	0.2	1
Surface Tension, $\sigma \times 10^3$ [J.m <sup>-2</sup> ]	800	600	74	20
$-d\sigma/dT \times 10^4$ [N.m <sup>-1</sup> .K <sup>-1</sup> ]	3	3	1.7	10 <sup>-4</sup>
Thermal Conductivity, $k$ [W.m <sup>-1</sup> .K <sup>-1</sup> ]	0.67	0.71	0.6	0.12
Thermal Capacity, $c_p \times 10^{-3}$ [J.kg <sup>-1</sup> .K <sup>-1</sup> ]	1.0	0.38	4.2	1.8
Thermal Diffusivity, $(\sigma = k/\rho c_p) \times 10^6$	2.0	34	0.14	0.07
Kinematic Viscosity, $\nu \times 10^6$ [m <sup>2</sup> .s <sup>-1</sup> ]	0.35	0.14	1	5
Prandtl Number, $Pr = \nu/a$	0.02	0.01	7	55

$$R=R(t,z,\theta,S(t),Q(t),\text{sample,furnace}) \quad (3)$$

with  $z_1(t) \leq z \leq z_2(t)$ . The problem to compute the temperature field corresponding to a given heating law is already a great task (Ref. 13).

- What are the internal motions created by bulk or surface forces.
- Which is the finally solidified structure (f.i. dopant distribution).

Now let us look from the other side and see what the LB theory really offers to the FZ research.

#### 4. RESULTS OF THE LIQUID BRIDGE MODEL

The LB model corresponds to the configuration sketched in Fig. 7, and a lot of work has been carried out on it (Ref. 14), which may be summarised as follows:

- Equilibrium shape and stability:
  - \* axisymmetric and non-axisymmetric:
- Internal motions and shape deformation
  - \* vibration (axial and lateral)
  - \* rotation (concentric and eccentric)
  - \* thermocapillarity (steady and oscillatory)
  - \* buoyancy
  - \* others (f.i. submerged jet).

Although the theoretical foundations of these studies are well known (Young-Laplace capillarity equation and Navier-Stokes equations), because of their non-linear behaviour, the solutions are difficult to guess, what, added to the great variety of boundary conditions of interest, makes a general analysis too difficult and one must resort to numerical computations (Ref. 15). But numerical solutions are obtained for a particular set of governing parameters that may be key to an experimenter looking at its checkout, but which are of little help to other persons interested to learn about LB behaviour in a broader scope, as happens for an investigator on floating zones. However, in absence of better analytical descriptions, a concrete numerical case-study may contribute to the understanding of a more general problem, and to check future theoretical models. Moreover, if the numerical computation solves some characteristic limit, its interest increases and may be a cornerstone to serve as a reference for more analytical work, that near some asymptotic limits tends to become more tractable.

In particular, the fluid-statics theory of axisymmetric liquid bridges held by surface tension forces and anchored to the edges of sharply-cut solid discs of radius  $R_1$  and  $R_2$ , predicts the outer shape deformation of an initially cylindrical liquid column when subjected to different axisymmetric disturbances quantified by the discs ratio  $K=R_1/R_2$ , the length ratio  $\Lambda=L/(2R_o)$  where  $R_o=(R_1+R_2)/2$ , the volume ratio  $v=V/R_o^3$ , an axial acceleration  $g$  corresponding to a Bond number  $Bo_R=\rho g R^2/\sigma$ , a centrifugal force measured by the Weber number  $We=\rho \Omega^2 R_o^3/\sigma$ , an axial harmonic vibration of nondimensional amplitude  $a=A/R_o$  and nondimensional pulsation  $\omega=[\rho(2\pi f)^2 R_o^3/\sigma]^{1/2}$ , where  $A$  and  $f$  are the dimensional amplitude and frequency, a non-uniform interfacial tension profile, etc.

An example of an interesting limit case is the maximum Bond number, now rescaled to  $Bo_L = \Delta \rho g L^2/\sigma$ , that an initially cylindrical bridge of reduced length  $L_r = L/(2\pi R_o)$  may sustain, a numerically-generated diagram of which is shown in

Fig. 8. This may be of great help when looking for asymptotic expressions like:

$$\left. \begin{aligned} Bo_L &\xrightarrow{L_r \rightarrow 1} \frac{16\pi^2}{9} (1-L_r)^{3/2} \\ Bo_L &\xrightarrow{L_r \rightarrow 0} 13,2 \end{aligned} \right\} \quad (4)$$

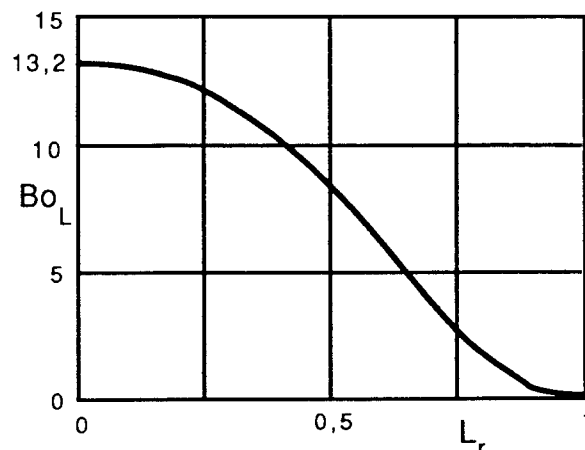


Fig. 8. Maximum axial acceleration,  $g$  (measured by the Bond number,  $Bo_L$ ) that an initially cylindrical liquid column anchored to equal solid discs of radius  $R_o$  and separated a distance  $L$ , can withstand.

The last limit in (4) can be expressed analytically also (Ref. 16). It is interesting to note that in both limits ( $L_r \rightarrow 1$  and  $L_r \rightarrow 0$ ) the meridian shape is antisymmetric with respect to midplane between discs, but it deforms deeper at the neck than it bulges at the belly for all intermediate values of  $L_r$ .

#### 5. CONCLUSIONS

The importance of the floating zone process and the multidisciplinary phenomena that there appear, demand a multidisciplinary effort to model it, and the liquid bridge theory can substantially contribute in this way.

The conditions under which the LB model may be applied to real FZ processes have been here analysed in detail.

Presently, theoretical and experimental research on LB is based on the application of some direct boundary conditions (f.i. known length and volume) which are not directly controllable in real FZ experiments (where pulling and heating laws are the primary variables). It can be easily appreciated that further work is needed trying to close the gap between basic LB research and its application to FZ processes, particularly in connection with the thermal and solutal fields.

#### ACKNOWLEDGEMENTS

Part of this work is being sponsored by the Spanish CICYT under Project No. ESP-88-0359.

#### REFERENCES

1. Eyer A, Leiste H & Nitsche R 1984, Crystal growth of silicon in Spacelab-1, *Proc. Vth European Symposium on Materials Sciences under Microgravity*, ESA SP-222, 173-181.

2. Martínez I & Eyer A 1986, Liquid bridge analysis of silicon crystal growth experiments under microgravity, *J. Crystal Growth*, 75, 535-544.
3. Eyer A, Leiste H & Nitsche R 1985, Floating zone growth of silicon under microgravity in a sounding rocket, *J. Crystal Growth*, 71, 173-182.
4. Kölker H 1984, Crystallisation of a silicon sphere, *Proc. Vth European Symposium on Materials Sciences under Microgravity*, ESA SP-222, 169-172.
5. Kölker H 1987, Crystallisation of a silicon sphere, in *Scientific Results of the German Spacelab Mission D1; Sahm, P.R., Jansen, R., Keller, M.H. (Eds.), DFVLR, Koeln, FRG*, 264-267.
6. Eyer A & Leiste H 1985, Striation-free silicon crystals by float-zoning with surface-coated melt, *J. Crystal Growth*, 71, 249-252.
7. Cröll A, Müller-Sebert W, Benz K W & Nitsche R 1991, Natural and thermocapillary convection in partially confined silicon melt zones, *Microgravity Sci. Technol.*, III/4, 204-215.
8. López-Díez J 1991, Low-Marangoni Low-Reynolds Numbers Capillary Flow Inside a Slender Liquid Bridge, *Microgravity Sci. Technol.*, III/4, 222-230.
9. Martínez I, Sanz A, Perales J M & Meseguer J 1988, Freezing of a long liquid column on the Texus-18 sounding-rocket flight, *ESA Journal*, 12, 483-489.
10. Monti R & Fortezza R 1991, The scientific results of the experiment on oscillatory Marangoni flow performed in telepresence on Texus-23, *Microgravity Quart.*, 1, 163-171.
11. González H, McCluskey F M J, Castellanos A & Barrero A 1989, Stabilisation of dielectric liquid bridges by electric fields in the absence of gravity, *J. Fluid Mech.*, 206, 545-561.
12. Martínez I 1988, Liquid bridge modelling of floating zone processing, in *Physicochemical Hydrodynamics and Interface Phenomena*, M.G. Velarde (Ed.), Plenum Press, 25-51.
13. Rivas D, Sanz J & Vázquez C 1992, Temperature field in a cylindrical crystal heated in a mono-ellipsoid mirror furnace, *J. Crystal growth*, 116, 127-136.
14. Martínez I, Haynes J M & Langbein D 1987, Fluid statics and capillarity, in *Fluid Sciences and Materials Sciences in Space*, H.U. Walter (Ed.), Springer-Verlag, 53-81.
15. Martínez I, Perales J M & Gómez M 1992, Effects of axial and centrifugal forces on the stability of liquid bridges, (in this Symposium).
16. Martínez I & Perales J M 1987, Bidimensional liquid bridges in a gravity field, *Acta Astronautica*, 15, 567-571.